

ROSAT PSPC OBSERVATIONS OF THE RICHEST ($R \geq 2$) ACO CLUSTERS

LAURENCE P. DAVID, WILLIAM FORMAN, AND CHRISTINE JONES

Harvard-Smithsonian Center for Astrophysics

60 Garden Street
Cambridge, MA 02138

Accepted by The Astrophysical Journal

ABSTRACT

We have compiled an X-ray catalog of optically selected rich clusters of galaxies observed by the PSPC during the pointed GO phase of the ROSAT mission. This paper contains a systematic X-ray analysis of 150 clusters with an optical richness classification of $R \geq 2$ from the ACO catalog (Abell, Corwin, and Olowin 1989). All clusters were observed within $45'$ of the optical axis of the telescope during pointed PSPC observations. For each cluster, we calculate: the net 0.5-2.0 keV PSPC count rate (or 4σ upper limit) in a 1 Mpc radius aperture, 0.5-2.0 keV flux and luminosity, bolometric luminosity, and X-ray centroid. The cluster sample is then used to examine correlations between the X-ray and optical properties of clusters, derive the X-ray luminosity function of clusters with different optical classifications, and obtain a quantitative estimate of contamination (i.e., the fraction of clusters with an optical richness significantly overestimated due to interloping galaxies) in the ACO catalog.

Due to the large field of view of the PSPC, many rich clusters were serendipitously observed during the GO phase of the ROSAT mission. Of the 150 clusters in our sample, 82 were observed serendipitously, and 68 were targeted observations. The overall detection rate of serendipitously observed clusters is quite high at 76%. However, the detection rate is sensitive to the optical properties of clusters, and the details of the optical selection process. For example, all serendipitously observed Bautz-Morgan Type I and I-II clusters are detected, while only 71% of Bautz-Morgan Type II, II-III, and III clusters are detected. Beyond $z \approx 0.1$, 83% of the observed Abell clusters are detected, compared to only 60% of southern ACO clusters. Due to the long integration times in pointed PSPC observations, the typical X-ray luminosity threshold for detection is quite low at $\sim 10^{43}$ ergs s^{-1} for clusters within $z=0.2$. This luminosity is more characteristic of an X-ray luminous group rather than a rich cluster. The nondetected clusters must therefore be either highly unrelaxed systems or have an optical richness that is significantly overestimated due to contamination by interloping galaxies. We show that the later possibility is more likely since low X-ray luminosity clusters are preferentially found in denser cluster environments compared with X-ray luminous clusters. This contrast in cluster environment makes low X-ray luminosity clusters more susceptible to galaxy contamination than luminous systems. The fraction of clusters less luminous than an X-ray luminous group is thus a direct quantitative measure of contamination in the ACO catalog. We also find that the X-ray luminosity function of Abell clusters is inconsistent with that of southern ACO clusters. Only by comparing $R \geq 2$ Abell clusters with $R \geq 3$ southern ACO clusters can we obtain consistency in their X-ray properties. This indicates that the optical richness of southern ACO clusters is overestimated by about one richness class.

Subject headings: galaxies: clusters: general

1. INTRODUCTION

X-ray observations of clusters of galaxies over the past 20 years have proven invaluable for determining many fundamental properties of clusters. Such observations provide essential diagnostics for constraining the history and dynamical evolution of individual clusters along with models governing the evolution of the universe as a whole. The ROSAT observatory (Trümper 1983), which was launched on June 1, 1990, has had a tremendous impact on our knowledge of clusters of galaxies. ROSAT conducted the first all-sky survey by an imaging X-ray telescope in 4 segments between July 1990 and Aug 1991. This survey produced two major X-ray catalogs of clusters: the ROSAT Brightest Cluster Sample (BCS; Ebeling *et al.* 1998) and the X-Ray Brightest Abell Cluster Sample (XBACS; Ebel-

ing *et al.* 1996). Aside from the 6 months during which the ROSAT All-sky Survey (RASS) was conducted, all other observing time was allocated to guest observers. The ROSAT PSPC carried out nearly 6000 observations during its 4 years of operation in the GO phase of the ROSAT mission. Excluding the shortest observations (integration times less than 50 seconds) and a series of observations that were used to fill in the ROSAT All-Sky Survey, leaves 5003 pointed PSPC observations that covered 16.5% of the sky. Of these, 4883 PSPC observations are now available to the public through, e.g., the HEASARC at GSFC. This archive contains a wealth of information about the X-ray properties of many astronomical objects. In this paper, we present the results of a systematic analysis of pointed PSPC observations of rich clusters of galaxies.

Cross-correlating the positions of optically rich clusters in the ACO catalog (Abell, Corwin, and Olowin 1989), with the ROSAT Master Observation Catalog shows that 882 ACO clusters were observed during the 5003 pointed PSPC observations that are presently available through the HEASARC. Most of these observations were serendipitous, and not requested pointings. The primary advantage of pointed PSPC observations compared with ROSAT all-sky survey (RASS) data, is the much longer integration time. The typical exposure time for a pointed PSPC observation is 10,000 seconds, compared with 400 seconds in the RASS. Of course, the main advantage of the RASS over the pointed PSPC phase is the nearly complete sky coverage. The longer integration times obtained during pointed PSPC observations have several advantages relevant to the data analysis: 1) lower flux limits for detection, 2) better discrimination between point-like and extended sources, and 3) less source confusion. For these reasons, we have compiled a catalog of the 150 optically richest ACO clusters (richness class $R \geq 2$) observed by the PSPC during the GO phase of the ROSAT mission.

This paper is organized in the following manner. In section 2, we present our cluster sample, data reduction techniques, and X-ray detection rates. We also discuss in §2 how the X-ray detection rates depend on the optical properties of rich clusters. In section 3 we compare the X-ray fluxes determined from pointed PSPC with those obtained from the RASS data for all clusters in common with our sample and the XBACS. Section 4 investigates correlations between the X-ray and optical properties of rich clusters. The X-ray luminosity function (both parametric and nonparametric) of the entire sample and several sub-samples (based on optical properties) is derived in section 5. Section 6 presents an investigation of contamination in the ACO catalog, and finally, the main results are summarized in section 7.

2. DATA REDUCTION

2.1. 2.1 The Sample

Our sample contains all ACO clusters with a richness class of $R \geq 2$ ($N_{gal} \geq 80$) that lie within $45'$ of the optical axis of a pointed PSPC observation. This selection criterion ensures that the central $1 h_{50}^{-1}$ Mpc of a cluster lies within the full PSPC field of view for all clusters beyond $z = 0.04$. We use the HEASARC Browse search engine to cross-correlate the cluster positions in the ACO catalog with the PSPC master observation log. This search produced 82 serendipitously observed ACO clusters and 68 targeted clusters (see Table 1). The mean exposure time for the 150 observed clusters is 9.6 ksec, which is approximately 25 times the mean exposure time in the RASS.

To determine if our sample is representative of the general optical properties of ACO clusters, we compare the distribution of optical richness (N_{gal}), Bautz-Morgan Type, Rood-Sastry Type, and distance class in Figure 1. Bautz-Morgan Types are available for 142 of the clusters in the PSPC sample and we compare their distribution with that of Abell's statistical sample (Leir and Van den Berg 1977). Rood-Sastry classifications and their relative abundances are available for all clusters in Abell's (1958)

TABLE 2
Comparison of Optical Properties (KS test results)

Property	Targeted	Serendipitous	Entire Sample
N_{gal}	0.0026	0.97	0.064
BM Type	3×10^{-5}	0.98	3×10^{-3}
RS Type	3×10^{-3}	0.87	0.01
D Class	4×10^{-6}	0.99	0.04

Notes: This table give the probability that the targeted, serendipitous, and entire PSPC samples were drawn from the same parent population of clusters as the ACO catalog, based on optical richness, Bautz-Morgan Type, Rood Sastry Type, and Distance class.

original catalog from Struble and Rood (1987). Figure 1 shows that the targeted observations are biased toward nearby, rich, Bautz-Morgan Type I, cD clusters, while the optical properties of the serendipitously observed clusters reflect the general properties of ACO clusters. This impression is confirmed using a KS test to determine the statistical significance of these differences (see Table 2). For example, Bautz-Morgan Type I clusters only comprise 3.4% of Abell's statistical sample, compared with 26% of the targeted observations of clusters. Due to the contrasting optical properties of the targeted and serendipitous samples, these samples will be analyzed separately below.

2.2. Analysis Techniques

All PSPC data are screened and reduced using the software package developed by Snowden *et al.* (1994) for the analysis of extended objects. The first 15 seconds of each observation interval is excluded due to possible aspect uncertainties while the target is being acquired. In addition, all time intervals with master veto rates greater than 170 cts s^{-1} are excised. Images, exposure maps, exposure corrected count rate images, and exposure corrected count rate error images are generated for the resulting good time intervals for each of 4 highest energy bands (R4-R7) covering the energy range 0.51-2.01 keV (hereafter 0.5-2.0 keV). The images are blocked to a scale of $15''$ per pixel. For clusters with multiple PSPC exposures (i.e., when the ACO cluster centroid is within the central $45'$ radius region of more than one PSPC observation), all observations are aligned and co-added.

Every 0.5-2.0 keV exposure corrected count rate image is then inspected for the presence of an extended source within one-third of an Abell radius around the optical position of the cluster given in ACO. If extended emission is detected (based on the PSPC PSF of a 5 keV thermal source at the appropriate angle off-axis) than the centroid of the X-ray emission determined by the PROS task *examine* is used as the center of the source circle. Since many of the clusters in this sample are among the X-ray brightest clusters in the sky, the X-ray identification is usually quite obvious. In observations without a detected extended source within one-third of an Abell radius, the center of the source circle is positioned at the ACO optical position. The total counts are then extracted using a circular source region with a radius of 1 Mpc in the rest

frame of the cluster, excluding the emission from all unresolved sources. The luminosity and angular distances are computed from measured redshifts, if available, otherwise, redshifts are estimated from the m_{10} vs. z relation given in Ebeling *et al.* (1996). All distant dependent quantities are computed assuming $H_0 = 50 \text{ km}^{-1} \text{ s}^{-1} \text{ Mpc}^{-1}$ and $q_0 = 0.5$. The background rate is determined from several regions in the same observation that are free of obscuration by the PSPC window support structure and beyond 3 Mpc of the cluster centroid. For the few low redshift clusters that fill the field of view (e.g., A426, A1367, A1656), a background rate of $3.5 \times 10^{-4} \text{ cts s}^{-1} \text{ arcmin}^{-2}$ is used, which is the median value in the remainder of the PSPC observations.

The net count rates and errors in the 0.5-2.0 keV energy band are then determined using the standard propagation of errors (see below). To convert from count rates to fluxes we use previously measured temperatures, if available, from David *et al.* (1993). Otherwise, we perform an iterative procedure to estimate the temperature based on the relation between X-ray luminosity and gas temperature given in David *et al.* The 0.5-2.0 keV and bolometric fluxes are determined assuming a Raymond thermal plasma model with the measured or estimated gas temperature, 30% solar abundance, and the galactic hydrogen column density along the line of sight toward the cluster from Stark *et al.* (1992). The resulting X-ray properties of the cluster sample are given in Table 1.

2.3. Sensitivity and Detection Rates

The flux limit for detecting extended sources depends on the source morphology, redshift, exposure time, and background rate. The net count rate of a cluster, R_s , is simply $R_s = R_t - R_b(A_s/A_b)$, where R_t and A_s are the total count rate and area in the source circle, and R_b and A_b are the background count rate and area in the background region. The error in R_s is then, $\sigma_s^2 = \sigma_t^2 + (A_s/A_b)^2 \sigma_b^2$. Figure 2 shows the 3σ flux limit for a source radius of 1 Mpc, a background rate of $3.0 \times 10^{-4} \text{ cts s}^{-1} \text{ arcmin}^{-2}$, and a typical background region with $A_b = 300 \text{ arcmin}^2$. Flux limits are shown for exposure times of 400 sec (typical of the RASS), 10 ksec (the mean in our sample), and 50 ksec (representative of some of the longest PSPC observations). Also shown in Figure 2 is the 3σ flux limit for a point source with no background in the source circle (9 net counts). As the redshift increases, A_s/A_b decreases, and the flux limit for an extended source approaches that of a point source. Figure 2 shows that typical flux limits in pointed PSPC observations are an order of magnitude below that possible in the RASS. The flux limit for detecting clusters at $z=0.3$ is approximately 30 times less than that of clusters at $z=0.02$. This corresponds to an increase in luminosity of only a factor of 10 between $z=0.02$ and 0.3, compared with a factor of 220 for point sources at the detection threshold. This shows that extended sources detected using a fixed physical source radius are much less affected by Malmquist bias than point sources.

The detection efficiency of the clusters in our sample is summarized in Table 3. Nearly all of the targeted clusters are detected (64/68). This is not surprising, since the X-ray flux of many of the targeted clusters was already known from previous X-ray missions and the requested exposure times guaranteed a detection. The overall

TABLE 3
Detection Rates

Sample	$z < 0.1$	$0.1 \leq z < 0.2$	$z \geq 0.2$	All Redshift
Targeted	33/34 (97%)	21/23 (91%)	10/11 (91%)	64/68 (94%)
Serendipitous	6/6 (100%)	40/53 (75%)	16/23 (70%)	62/82 (76%)
Abell	21/22 (95%)	54/64 (84%)	22/28 (79%)	97/114 (85%)
Southern ACO	18/18 (100%)	7/12 (58%)	4/6 (67%)	29/36 (80%)

detection rate of serendipitous clusters is also quite high at 76%. There is also a slight difference between the detection rate of Abell (83%) and southern ACO (60%) clusters beyond $z \approx 0.1$. Table 4 shows that all of the nondetected serendipitously observed clusters have late Bautz Morgan Types. All serendipitously observed clusters with Bautz Morgan Types of I or I-II, or $R \geq 2$ are detected. The mean upper limit on the 0.5-2.0 keV luminosity for the nondetected serendipitously observed clusters is $1.4 \times 10^{43} \text{ ergs s}^{-1}$, which is comparable to the X-ray luminosity of the NGC 5044 group of galaxies (David *et al.* 1994). Optically, the NGC 5044 group does not even qualify as a dense Hickson group. Thus, the nondetected clusters are either dynamically unrelaxed multi-component systems, or have an optical richness that is significantly over estimated due to intervening galaxies. We discuss the effects of contamination in the ACO catalog in § 6.

For comparison, Ebeling *et al.* (1993) cross-correlated the positions of sources detected by SASS in the individual RASS scans with the optical cluster positions in ACO, and found that 22% of $R \geq 1$ clusters were detected above a flux limit of $7 \times 10^{-13} \text{ ergs cm}^{-2} \text{ s}^{-1}$ in the 0.1–2.4 keV bandpass. Briel and Henry (1993) analyzed the RASS data on a complete sample of Abell clusters within a 561 square degree region at high galactic latitudes with an average exposure time of 660 sec. They detected 46% at a significance level for existence greater than 3σ , and computed X-ray fluxes at better than 3σ for 36%. The greater detection rate in pointed observations is simply due to the greater exposure times. However, still longer observations will not necessarily increase the detection rate substantially, since many of the clusters not detected in pointed observations may not be physically bound systems.

3. COMPARISON WITH XBACS

Ebeling *et al.* (1996) compiled a sample of 242 ACO clusters (XBACS) detected in the RASS with unabsorbed 0.1-2.4 keV fluxes greater than $5.0 \times 10^{-12} \text{ ergs cm}^{-2} \text{ s}^{-1}$. There are 42 clusters in common between our two samples. To make a direct comparison between the analysis of the

TABLE 4
Detection Rates of Serendipitous Observed Clusters

Bautz-Morgan Type	R=2	$R \geq 3$
I, I-II	8/8	1/1
II, II-III, III	41/59	8/10

pointed PSPC observations and the RASS data, we have to account for differences in the energy bandpass and extraction radius. The uncorrected 0.1-2.4 keV count rates given in Ebeling *et al.* are derived from the VTP source detection algorithm, which essentially gives the net count rates within a radius of r_{VTP} . The corrected count rates include the source flux beyond r_{VTP} (assuming a spherically symmetric King model with $\beta = 2/3$ and a core radius determined from the data) and a statistical correction for the flux from unresolved point sources. The final unabsorbed 0.1-2.4 keV fluxes are then derived from the corrected count rates, the galactic hydrogen column densities in Stark *et al.* (1992), and measured temperatures, if available, from David *et al.* (1993). If the gas temperature is unknown, then the temperature is estimated from the X-ray luminosity-temperature relation given in White, Jones & Forman (1997). The best quantity to use for comparison between our two samples is the unabsorbed flux, since it is derived from the same values for the hydrogen column density. For a Raymond thermal plasma model, the ratio of the unabsorbed flux between 0.5-2.0 keV and 0.1-2.4 keV is also very insensitive to gas temperature and only varies from 0.60 for a 2 keV cluster to 0.62 for a 10 keV cluster. We therefore use a conversion factor of 0.61 for all clusters. To interpolate from the total flux in Ebeling *et al.*, to the flux within the central 1 Mpc, we assume that all clusters can be represented by a spherically symmetric β model with $\beta = 2/3$, and core radii between 100 and 250 kpc. For core radii of 100 kpc and 250 kpc, 91% and 76% of the total flux is contained within the central 1 Mpc, respectively.

A comparison of the unabsorbed 0.1-2.4 keV fluxes in Ebeling *et al.* with the unabsorbed 0.5-2.0 keV fluxes derived from the pointed PSPC observations is shown in Figure 3. The error bars in Figure 3 only include the quoted errors on the count rates. The dashed lines indicate exact agreement for core radii of 100 and 250 kpc. This figure shows that there is excellent agreement between the analysis of the RASS data presented in Ebeling *et al.* with the analysis of the pointed PSPC observations presented here. Only 2 clusters (A2069 and A2151) have measured fluxes that differ at more 3σ ; however, both of these are double clusters, and the assumption of spherical symmetry used to interpolate between the two flux measurements is certainly inaccurate.

Using the conversion factors given above, the XBACS flux limit corresponds to a 0.5-2.0 keV flux limit within the central 1 Mpc of 2.5×10^{-12} ergs cm^{-2} s^{-1} . There are three clusters in our sample (A2034, A3223, and A3301) with fluxes greater than this value (see Table 3). A2034 was removed from the XBACS sample due to possible contamination from an AGN. The longer (7.0 ksec) pointed observation of A2034 shows that the dominant X-ray component is extended. A3223 has a SASS count below the threshold of 0.1 cts/s required for inclusion in the XBACS.

Morphologically, this is a complicated cluster with several point sources embedded within extended emission. A3301 also has a SASS count rate less than 0.1 cts/s. Overall, there are 45 clusters above the XBACS flux limit in our sample and 42 of these are included in the XBACS. This implies that the XBACS is 93% complete, which is within the 80% completeness estimate given in Ebeling *et al.*

4. CORRELATIONS BETWEEN X-RAY AND OPTICAL PROPERTIES

A correlation between X-ray luminosity and cluster richness has been found from Ariel V, Uhuru, HEAO-1, Einstein, and Exosat observations (McHardy 1978; Jones and Forman 1978; Johnson *et al.* 1983; Edge and Stewart 1991; Burg *et al.* 1994). There have also been claims for and against a correlation between L_x and Bautz-Morgan Type (Bahcall 1977; McHardy 1978; Jones and Forman 1978; Johnson *et al.* 1983). Most of these early samples contained too few clusters to isolate independent correlations between richness and Bautz-Morgan Type, and only contained the most X-ray luminous clusters.

A scatter plot of L_x versus cluster richness, N_{gal} , is shown in Figure 4. Different symbols are used to indicate early Bautz-Morgan Type clusters (I and I-II) and late Bautz-Morgan Type clusters (II, II-III, and III). For comparison, we also show in Figure 4, the 0.5-2.0 keV luminosity of the NGC 5044 group. While there is a significant amount of scatter in this plot, the generalized Kendall's τ test (which uses the information contained in the nondetections) gives a probability of only 3×10^{-4} that L_x and N_{gal} are uncorrelated for the entire sample, and a probability of $< 10^{-4}$ for the serendipitously observed sample. Figure 4 shows that the X-ray luminosity of R=2 clusters varies by a factor of 500, and completely spans the range from small groups, to the most X-ray luminous clusters.

The significance of the correlation between L_x and N_{gal} actually depends on the Bautz-Morgan Type. Examination of Figure 4 shows that the X-ray luminosity of early Bautz-Morgan Type clusters appears to be independent of cluster richness. This impression is confirmed using the generalized Kendall's τ test, which gives an 83% probability that L_x and N_{gal} are uncorrelated for the early Bautz-Morgan Type clusters. This indicates that the well know correlation between X-ray luminosity and richness primarily pertains to late Bautz-Morgan Type clusters.

Based on the entire sample of $R \geq 2$ clusters, the X-ray luminosity is also strongly correlated with the Bautz-Morgan Type. There is only a 2×10^{-4} probability that L_x and Bautz-Morgan Type are uncorrelated for the entire sample, and a probability of 2×10^{-3} for the serendipitously observed sample. To differentiate between the dependence of L_x on cluster richness and Bautz-Morgan Type, we show scatter plots of the X-ray luminosities and Bautz-Morgan Types for just the $R = 2$ clusters in Figure 5. While there is significant scatter in L_x for a given Bautz-Morgan Type, there is a systematic decline in L_x between Type I and Type III clusters. The median X-ray luminosity of the Type III clusters is almost an order of magnitude less than that of early Bautz-Morgan Type clusters. Using the nonparametric logrank test (which uses the information contained in the upper-limits), the probability that the early Bautz-Morgan Type clusters are culled from the same parent population as the late Bautz-Morgan

Type clusters is less than 10^{-4} .

These results show that the X-ray luminosity of clusters is just as strongly correlated with Bautz-Morgan Type as with cluster richness. For a given cluster richness, the X-ray luminosity of early Bautz Morgan Type clusters is greater than late Bautz-Morgan Type clusters. This may indicate that cD clusters are denser and more evolved systems, or that the cluster richness in late Bautz-Morgan Type clusters is overestimated due to a greater contamination of interloping galaxies (see § 6).

5. LUMINOSITY FUNCTION

5.1. Non-Parametric

We use the Kaplan-Meier estimator (see, e.g., Feigelson & Nelson 1985) to derive the non-parametric representation of the luminosity function. Clusters at low galactic latitude ($|b| < 20^\circ$) and beyond $z = 0.25$ are excluded from this analysis. The resulting 0.5-2.0 keV luminosity functions for the serendipitous and targeted samples are shown in Figure 6a. It is obvious from this figure that the targeted observations are biased toward X-ray luminous clusters. Based on a logrank test, the probability that the targeted and serendipitous samples were drawn from the same parent population is only 3×10^{-4} . There is also a significant difference between the X-ray luminosity function of Abell and southern ACO clusters (see Figure 6b). A logrank test gives a probability of only 9×10^{-3} that the northern and southern samples were drawn from the same parent population. This probability increases slightly to 0.015 if we restrict the comparison to serendipitously observed clusters. If we only include $R \geq 3$ clusters from the southern ACO catalog, then the probability increases significantly to 23%. These tests show that the richness of southern ACO clusters is overestimated with respect to northern Abell clusters by approximately 1 richness class. This will be discussed further in § 6.

In the previous section we, presented scatter plots of X-ray luminosity vs. cluster richness and Bautz-Morgan Type. While there are significant correlations between these quantities, there is a great deal of scatter in the plots. The differences between the X-ray luminosities of clusters as a function of richness and Bautz-Morgan Type are more impressive after compiling luminosity functions. Figure 6c compares the luminosity function of $R=2$ clusters with $R \geq 3$ clusters. A logrank test gives a probability of 7×10^{-3} that these clusters were culled from the same population. Figure 6d compares the luminosity function of early Bautz-Morgan Type clusters with late Bautz-Morgan Type clusters. A logrank test gives a probability of 9×10^{-4} that these clusters were culled from the same population, which is slightly more significant than the difference between richness class.

5.2. Normalization of the Luminosity Function

To properly normalize the luminosity functions, we need to determine the volume surveyed as a function of X-ray luminosity for each sub-sample. For a completely random X-ray sampling of ACO clusters, the proper normalization of the luminosity function is the volume surveyed in the ACO catalog, or equivalently, the number density of ACO clusters. Scaramella *et al.* (1991) calculated the co-moving number density of $R \geq 1$ Abell and southern ACO clusters

to be $8.7 \times 10^{-6} \text{ h}^3 \text{ Mpc}^{-3}$, and $12.5 \times 10^{-6} \text{ h}^3 \text{ Mpc}^{-3}$, respectively. Weighting these number densities by the solid angles surveyed in the Abell (4.47 Sr) and southern ACO catalog (2.77 Sr), and the fraction of $R \geq 2$ clusters relative to $R \geq 1$ clusters in the two catalogs, gives an average co-moving number density of $3.6 \times 10^{-7} \text{ h}_{50}^3 \text{ Mpc}^{-3}$ for $R \geq 2$ clusters.

The dependence of the volume surveyed on the X-ray luminosity of clusters in the targeted sample can be determined through a comparison with XBACS (Ebeling *et al.* 1996). The XBACS contains all ACO clusters detected in the RASS with 0.1-2.4 keV fluxes greater than $5.0 \times 10^{-12} \text{ ergs cm}^{-2} \text{ s}^{-1}$. For this flux limit, XBACS should be volume limited within $z \leq 0.25$ for clusters more luminous than $1.5 \times 10^{45} \text{ ergs s}^{-1}$ in the 0.1-2.4 keV bandpass. There are 9 such clusters in the XBACS with $R \geq 2$, and 8 of these are contained in our targeted sample. This indicates that our targeted sample is nearly volume limited for $R \geq 2$ clusters, within $z = 0.25$, and more luminous than $\sim 10^{45} \text{ ergs s}^{-1}$. A lower limit to the luminosity function at the high luminosity end of the targeted sample can thus be obtained by using the volume within $z = 0.25$ and within the solid angle surveyed in the ACO catalog. Figure 7 compares the luminosity function of the volume normalized targeted sample (correcting for a factor of 9/8 for incompleteness) with the luminosity function of the ACO number density normalized serendipitous sample (correcting for the fraction of ACO clusters included in the targeted sample). This figure shows that the targeted sample is roughly 5% volume complete at low luminosities. As a consistency check, the completeness of the targeted sample at low luminosities should just be the fraction (8%) of all $R \geq 2$ ACO clusters for which pointed PSPC observations were carried out successfully. Figure 7 shows that the survey volume increases with luminosity in the targeted sample, and decreases with luminosity in the serendipitous sample. Thus, the true X-ray luminosity function of $R \geq 2$ clusters should connect the low luminosity end of the ACO number density normalized serendipitous sample with the high luminosity end of the volume normalized targeted sample.

The main goal of this section is to derive the X-ray luminosity function of an optically selected sample of clusters. We have already shown how the optical properties of clusters in the PSPC sample differ those in the from ACO catalog. However, we can still construct a luminosity function from the PSPC observations which reflects the luminosity function of a randomly selected sample of ACO clusters. To accomplish this, we implement a slight modification to the Kaplan-Meier estimator, which is given by:

$$\Phi(L_x) = 1 - \prod_{i, L_{x,i} > L_x}^n (1 - d_i/n_i)$$

where d_i equals the number of detections at $L_{x,i}$ and n_i is the number of clusters with $L_x \leq L_{x,i}$. To correct for biases in the optical properties of the PSPC sample, we write n_i as:

$$n_i = \sum_{j \leq i} f_j^{-1}$$

where f_j is the under-sampling of a cluster with an X-ray

luminosity of $L_{x,j}$ based on its richness and Bautz-Morgan Type. For example, there are 35 clusters in the ACO catalog with $R = 2$ and Bautz Morgan Type I, compared to 12 such clusters in the PSPC sample. Thus, each such cluster in the PSPC sample is treated as 2.9 clusters in the construction of the X-ray luminosity function. Defined in this way, we can construct an X-ray luminosity function of ACO clusters with the proper abundance of each richness class and Bautz-Morgan Type. The resulting 0.5-2.0 keV and bolometric luminosity functions are shown in Figure 8. By using the above modification to the Kaplan-Meier estimator, we have successfully generated a luminosity function that agrees with the ACO number density normalized serendipitous sample at low luminosities, and the volume normalized targeted sample at high luminosities.

5.3. Parametric Luminosity Function

Cluster X-ray luminosity functions derived from HEAO-1 (Kowalski, Ulmer, and Cruddace 1983), Einstein (Burg *et al.* 1994), and ROSAT (Ebeling *et al.* 1997) observations are best fit by a Schechter luminosity function, given by:

$$\Phi(L)dL = N^* \left(\frac{L}{L^*}\right)^{-\alpha} \exp\left(-\frac{L}{L^*}\right) d\left(\frac{L}{L^*}\right)$$

We fit our sample using the detections and bounds technique described in Avni & Tananbaum (1986). The normalization is adjusted in the fitting procedure to satisfy the observed number density of $R \geq 2$ clusters ($N^* = n(R \geq 2)/\Gamma(1 - \alpha)$). The maximum likelihood method gives $\alpha = 0.29(0.25 - 0.33)$ and $L^* = 3.2(2.7 - 3.7) \times 10^{44}$ ergs s^{-1} for the 0.5-2.0 keV luminosity function and $\alpha = 0.47(0.43 - 0.51)$ and $L^* = 2.0(1.6 - 2.4) \times 10^{45}$ ergs s^{-1} for the bolometric luminosity function. Errors are given at the 90% confidence limit for one interesting parameter ($\chi_{min}^2 + 2.71$).

5.4. Comparison With Previous Luminosity Functions

The earliest cluster X-ray luminosity functions were derived from Uhuru, Ariel V, and HEAO-1 data (Schwartz 1978; McHardy 1978; Kowalski, Ulmer, and Cruddace 1983). The main differences between these early cluster samples and the pointed PSPC sample are the improved sensitivity and low energy coverage of the PSPC, which increases the efficiency of detecting low luminosity, cool clusters. An examination of the the Ariel V and Uhuru catalogs (compiled by Jones and Forman 1978) and the HEAO-1 catalog (Kowalski *et al.* 1984) shows that the least luminous $R \geq 2$ cluster detected in these early X-ray missions was A1367. The X-ray luminosity of A1367 is only slightly below the mean in our larger sample (48th percentile). While A1367 was considered an unusually low luminosity rich cluster based on the early X-ray missions,

our sample shows that the X-ray luminosity of A1367 is quite representative of $R \geq 2$ clusters.

Burg *et al.* (1994) compiled a sample of 212 Abell clusters observed by the Einstein IPC and calculated separate luminosity functions for $R = 0$, $R = 1$, and $R \geq 2$ clusters. The X-ray luminosities in Burg *et al.* are derived from the net 0.5-4.5 keV emission within 1 Mpc in the rest frame of the clusters. Assuming a source spectrum of $kT = 5$ keV and a galactic hydrogen column density of $N_H = 3 \times 10^{20}$ cm^{-2} gives a conversion factor of 1.8 between the IPC and PSPC luminosities. A summary of the main X-ray properties of the PSPC and IPC samples is given in Table 5. While the high luminosity end of the luminosity functions are in good agreement (above the 25th percentile), the PSPC sample has a much greater fraction of low luminosity clusters. There are 16 clusters in the PSPC sample less luminous than the least luminous cluster in the IPC sample, and the median luminosity in the PSPC sample is a factor of 2.5 less than that in the IPC sample (after correcting for bandpass effects). Since the IPC sample only contains 28 $R \geq 2$ clusters, Burg *et al.* were unable to constrain α and L^* independently and choose to fix $\alpha = 0.4$ in their fitting procedure. This value was chosen based on the X-ray luminosity function of optically less rich clusters. Our best fit value of α is slightly less, but within the 90% errors of the less rich clusters in Burg *et al.* The IPC sample consists mostly of targeted observations which produces the agreement with the PSPC sample at high luminosities. The disagreement between the IPC and PSPC luminosity functions at low luminosities arises from the large fraction of serendipitously observed clusters in the PSPC sample.

The ROSAT Brightest Cluster Sample (BCS) consists of all clusters in the northern hemisphere ($\delta \geq 0^\circ$, $|b| \geq 20^\circ$) that are detected in the ROSAT all-sky survey above a flux limit of 4.4×10^{-12} ergs cm^{-2} s^{-1} (Ebeling *et al.* 1998). The BCS includes ACO clusters, Zwicky clusters, and X-ray bright extended sources identified by the SASS. In addition, the BCS includes all clusters detected serendipitously with the VTP algorithm within a 2° square region around all X-ray bright ACO or Zwicky clusters, as well as around all X-ray bright extended sources detected by the SASS in the study region. In a separate paper, Ebeling *et al.* (1997) fit a Schechter function to all clusters in the BCS within $z = 0.3$. The results of their fitting procedure are summarized in Table 5 for the 0.5-2.0 keV bandpass. At luminosities above 3×10^{44} ergs s^{-1} there is good agreement between the BCS and PSPC samples, and the two estimates of L^* are consistent (after adjusting L^* in the BCS to give the flux within 1 Mpc). This probably results from the correlation between cluster richness and X-ray luminosity, which ensures that an optically selected sample of the richest ACO clusters will necessarily contain a large fraction of the most X-ray luminous clusters. At low luminosities, however, the luminosity functions of the BCS and PSPC samples are very different. The luminosity function of the BCS continues to rise at low luminosities while the PSPC sample essentially turns over, due to the lack of low X-ray luminosity $R \leq 2$ clusters in the PSPC sample. There is also good agreement at low luminosities between the luminosity function of the BCS and a sample of optically selected poor clusters (Burns *et al.* 1996). The steep luminosity functions of the BCS and the poor

TABLE 5
Comparison of X-Ray Luminosity Functions

Sample	L_{min} (ergs s ⁻¹)	75% (ergs s ⁻¹)	L_{median} (ergs s ⁻¹)	25% (ergs s ⁻¹)	L^* (ergs s ⁻¹)	α
PSPC	4.5×10^{42}	3.3×10^{43}	7.6×10^{43}	2.1×10^{44}	$(3.2 \pm 0.5) \times 10^{44}$	0.29 ± 0.04
IPC	1.5×10^{43}	8.4×10^{43}	1.9×10^{44}	3.9×10^{44}	$(4.3 \pm 0.6) \times 10^{44}$	0.4 (fixed)
BCS	3.3×10^{42}	6.9×10^{43}	1.8×10^{44}	4.5×10^{44}	$(5.7 \pm 1.1) \times 10^{44}$	1.85 ± 0.09
BH93	3.0×10^{43}	3.5×10^{43}	5.5×10^{43}	1.5×10^{44}	-	-

Notes: The IPC and BH93 luminosities have been converted to the 0.5-2.0 keV bandpass for comparison with the PSPC and BCS samples. Errors are given at the 90% confidence level for the PSPC sample, and at the 68% confidence level for the IPC and the BCS samples. The percentiles give the fraction of clusters more luminous than a given X-ray luminosity.

cluster samples cannot extend to arbitrarily low luminosities since the integrated luminosity of a Schechter function diverges if $\alpha > 1$. This requires that the composite luminosity function of clusters, groups, and galaxies must turn over at lower luminosities.

Finally, we compare our luminosity function with a complete sample of 145 ACO clusters observed at high galactic latitudes during the RASS (Briel and Henry 1993). To make a direct comparison with our sample, we extracted the 47 clusters from the Briel and Henry paper with $R \geq 2$, and used the Kaplan-Meier estimator to derive a non-parametric representation of the luminosity function. The results are summarized in Table 5. Briel and Henry give X-ray luminosities in the 0.5-2.5 keV bandpass, which requires a conversion factor of approximately 0.80. Examination of Table 4 shows that there is virtually no difference between these two estimates of the X-ray luminosity function of $R \geq 2$ clusters, even through the selection effects are quite different. This comparison shows that our method of correcting for bias in the pointed PSPC sample produces a luminosity function in good agreement with a purely random sampling. Due to the greater sensitivity of pointed PSPC observations compared to the RASS, our cluster sample spans a factor of 350 in X-ray luminosity compared to a factor of 20 in the Briel and Henry sample.

6. CONTAMINATION IN THE ABELL AND ACO CATALOGS

The identification of clusters from optical surveys is complicated by the presence of foreground and background galaxies and clusters. There have been many estimates of the fraction of clusters in the Abell and ACO catalogs that are significantly affected by contamination (Lucey 1983; Frenk *et al.* 1990; Struble and Rood 1991; van Haarlem, Frenk, & White 1997) and these estimates vary from 3-40%. Most of these contamination estimates are based on $R \geq 1$ clusters. Lucey estimated that contamination in $R \geq 2$ clusters is less significant by a factor of approximately 3. Since the emissivity of the hot gas in clusters scales as n_e^2 , X-ray observations are much less affected by contamination. The large number of ACO clusters observed during pointed PSPC observations permits an accurate assessment of contamination in these catalogs. The main results of sections 2 and 5 relevant to this issue are: 1) 97% of targeted Abell and southern ACO clusters and 100% of serendipitously observed clusters with $z < 0.1$ are detected, 2) at larger redshifts, 83% of Abell clusters, 75% of serendipitously observed clusters, and 60% of southern ACO clusters are detected, 3) all Bautz-Morgan Type I

and I-II clusters are detected (including 9 serendipitously observed clusters), 4) the X-ray luminosity function of $R \geq 2$ Abell clusters is significantly different than that of $R \geq 2$ southern ACO clusters, 5) the luminosity function of $R \geq 3$ southern ACO clusters is comparable to that of $R \geq 2$ Abell clusters.

These results indicate that the presence of a cD galaxy is a very reliable indication of a dense galactic and gaseous environment. The different X-ray luminosity functions for the Abell and southern ACO catalogs indicate that the optical richness of southern clusters is overestimated by about one richness class. This result is in agreement with Scaramella *et al.* (1991) who found "a tendency for rich clusters ($R \geq 2$) to be classified richer in ACO than in Abell," by comparing the galaxy counts of clusters in the overlap region between the two studies. This discrepancy is probably due to the different types of plates and the background subtraction techniques used in the two studies. Abell visually searched the 103a-E red plates of the Palomar Sky Survey to produce his original 1958 catalog, while UK 1.2m Schmidt telescope IIIa-J plates, which are blue-yellow sensitive, were used to compile the ACO catalog. Abell also derived the galaxy background from the same plate in a region apparently "free of clusters," while a global galaxy background was used in the generation of the ACO catalog. Since many clusters are located within superclusters and large scale filaments, the use of a global background can artificially increase the estimated richness of a cluster.

There are 34 clusters in our sample with $L(0.5 - 2.0 \text{ keV}) < 3.0 \times 10^{43} \text{ ergs s}^{-1}$. Of these, 22 are in Abell's statistical sample and 12 are in the southern ACO catalog. These clusters are good candidates for significant contamination since this luminosity is comparable to the luminosity of a dense group and a factor of 50 less than the most X-ray luminous clusters. While the exact degree of contamination is difficult to estimate, a reduction of approximately 2 richness classes may be appropriate for these clusters. Of the 22 clusters in the Abell statistical catalog, 2 (A1186 and A2198) are members of superclusters identified by West (1989), 2 (A1515 and A1607) are members of supercluster candidates in Batuski and Burns (1985), and A1566 is listed as a candidate for contamination in Struble and Rood (1991). Of the remaining 17 Abell clusters, only A536 has a measured redshift low enough ($z \lesssim 0.1$) to be included in present supercluster catalogs. Five of the low luminosity clusters (A968, A998, A1005, A1046, A1049) are contained within two nearby PSPC pointings (40' sep-

aration). Since the measured redshifts of these clusters are all between 0.190-0.203, they are probably members of a supercluster. Of the 12 low luminosity clusters in the southern ACO catalog, 2 (A3559 and A3566) are members of the Shapley supercluster and one (A3818) is listed as a supercluster candidate in Batuski *et al.* (1995). Of the remaining 9, only A3093 has a measured redshift that is less than 0.1. There is thus good evidence that a large fraction of the low luminosity clusters are members of superclusters and may be subject to significant contamination.

We are primarily concerned about the level of possible contamination in the low X-ray luminosity sample, and not whether these systems are part of a physically bound supercluster. For the former, we only need to search for nearby clusters with similar values of m_{10} , for the later, redshift surveys are required. We have calculated the angular separation of the nearest neighboring ACO cluster for all clusters in the PSPC sample. Only clusters with similar values of m_{10} ($\Delta m_{10} \leq 0.2$) are considered as possible sources of contamination. In figure 7, we plot the cumulative distribution of angular separations for low and high X-ray luminosity clusters. It is obvious from this figure that low X-ray luminosity clusters have an excess of nearby rich clusters compared with their more X-ray luminous counterparts. Seventy percent of low luminosity clusters have a neighboring cluster within 1° , compared to only 35% of more X-ray luminous clusters. A KS test only gives a 3×10^{-3} probability that these two distributions were drawn from the same population. It is worth noting that at a redshift of $z \sim 0.1$, an Abell radius ($1.5h^{-1}$) corresponds to about 20 arcminutes. Thus, the presence of a neighboring cluster within 1° certainly increases the possibility of contamination. This analysis shows that the optical richness of the low X-ray luminosity clusters is probably overestimated. Also, the large observed scatter between the X-ray luminosity and optical richness of clusters (see Figure 4) is probably due to varying degrees of contamination and not due to intrinsic variations between the X-ray properties of comparably rich clusters.

We can give a rough quantitative estimate of the fraction of clusters in the Abell and southern ACO catalogs that suffer from significant contamination (approximately 2 richness classes) as the fraction of serendipitously observed clusters with $L(0.5-2.0 \text{ keV}) < 3.0 \times 10^{43} \text{ ergs s}^{-1}$. This gives 20% and 35% for the Abell and southern ACO clusters. The larger fraction for the ACO clusters reflects the systematic off-set of 1 richness class previously mentioned.

7. SUMMARY

Over the next decade a host of new X-ray telescopes will be launched into orbit (e.g., AXAF, XMM, Spectrum X-Gamma, Astro-E, ABRIXAS). However, with the exception of ABRIXAS, none of these telescopes will carry out an all sky survey or have a detector with as large a field of view as the PSPC. Thus, for the near future, the ROSAT PSPC data archive will remain the prime database for searching fairly deep X-ray exposures of a substantial fraction of the sky. In this paper, we present a systematic data analysis of the 150 optically richest clusters observed by the PSPC during the GO phase of the ROSAT mission (i.e., richness class 2 or greater in the ACO catalog). Due to the long exposure times in

pointed PSPC observations, the detection threshold in most observations is comparable to an X-ray luminous group ($L(0.5-2.0 \text{ keV}) \sim 3 \times 10^{43} \text{ ergs s}^{-1}$). Undetected clusters must therefore be either highly unrelaxed or physically unbound systems (i.e., have an optical richness that is significantly overestimated due to contamination by intervening galaxies). The depth of this sample provides tight constraints for comparing the X-ray and optical properties of rich clusters, deriving luminosity functions, and determining the significance of galaxy contamination in the ACO catalog.

The detection probability of an ACO cluster is strongly dependent on its optical properties. All serendipitously observed Bautz Morgan Type I and I-II clusters are detected in PSPC observations, while only 71% of later Bautz Morgan Type clusters are detected. This result shows that the presence of a central dominant galaxy is a very reliable diagnostic for dense galactic environments. The PSPC cluster sample shows a strong correlation between X-ray luminosity and optical richness. For a given optical richness, there is also a correlation between X-ray luminosity and Bautz Morgan Type, with Bautz Morgan Type I clusters being the most luminous. We also find that the X-ray luminosity of Bautz-Morgan Type I clusters is independent of cluster richness, at least for $R \geq 2$ clusters.

There are also some discrepancies between the X-ray properties of clusters in the Abell and southern ACO catalogs. The X-ray luminosity function of $R \geq 2$ clusters in Abell's catalog is inconsistent with that of $R \geq 2$ clusters in the southern ACO catalog. However, the X-ray luminosity function of $R \geq 3$ clusters in the southern catalog is consistent with $R \geq 2$ clusters in the northern catalog. This indicates that there is a systematic offset of approximately 1 richness class between the northern and southern catalogs, in agreement with the results of Scaramella *et al.* (1991). The level of contamination by intervening galaxies in the Abell and ACO catalogs can be estimated as the fraction of clusters with X-ray luminosities less than $3.0 \times 10^{43} \text{ ergs s}^{-1}$ (typical of an X-ray luminous group). Using this criterion, we find that 20% of Abell clusters and 35% of southern ACO clusters suffer from significant contamination (at least 2 richness classes). The use of a global rather than a local galaxy background in ACO can explain the higher richness classification and greater level of contamination compared with the Abell catalog. Essentially all of the low redshift ($z < 0.1$), low X-ray luminosity clusters reside within superclusters. We also show that 70% of low luminosity clusters ($L(0.5-2.0 \text{ keV}) < 3.0 \times 10^{43} \text{ ergs s}^{-1}$) have a neighboring ACO cluster with comparable galaxy magnitudes ($\Delta m_{10} \leq 0.2$) within an angular separation of 1° , while only 35% of more luminous clusters have a similar ACO cluster within 1° .

The next generation of X-ray telescopes will acquire a great deal of detailed information on clusters of galaxies (e.g., gas temperatures, abundance of heavy elements, and small scale substructure) which will complement the PSPC observations and further our basic understanding of the formation and evolution of rich clusters.

We are grateful to the referee, H. Ebeling, for a very thorough reading of an early version of this paper and providing us with the percentiles on the X-ray luminosity function of the BCS given in Table 5. This research was

supported by NASA Grants NAG5-2745 and NAS8-39073.

REFERENCES

- Abell, G.O. 1958, *ApJS.*, 3, 211.
 Abell, G.O., Corwin, H.G., & Olowin, R.P. 1989, *ApJS.*, 70, 1.
 Avni, Y., Soltan, A., Tananbaum, H., & Zamorani, G. 1980, *Ap.J.*, 238, 800.
 Bahcall, N.A. 1977, *ApJ Lett.*, 217, L77.
 Batuski, D.J., & Burns, J.O. 1985, *AJ*, 90, 1413.
 Batuski, D.J., Maurogordato, S., Balkowski, C., & Olowin, R.P. 1995, *AA*, 294, 677.
 Briel, U.G., & Henry, J.P. 1993, *AA*, 278, 379.
 Burns, J.O., Ledlow, M.J., Loken, C., Klypin, A., Voges, W., Bryan, G.L., Norman, M.L., & White, R.A. 1996, *ApJ*, 467, L49.
 Burg, R., Giacconi, R., Forman, W., & Jones, C. 1994, *Ap.J.*, 422, 37.
 David, L.P., Slyz, A., Jones, C., Forman, W., Vrtilik, S., & Arnaud, K. 1993, 412, 479.
 David, L.P., Jones, C., Forman, W., & Daines, S. 1994, *Ap.J.*, 428, 544.
 Ebeling, H., Voges, W., Böhringer, H., & Edge, A.C. 1993, *AA*, 274, 360.
 Ebeling, H., Voges, W., Böhringer, H., Edge, A.C., Huchra, J.P., & Briel, U.G. 1996, *MNRAS*, 281, 799.
 Ebeling, H., Edge, A.C., Fabian, A.C., Allen, S.W., and Crawford, C.S., & Böhringer, H. 1997, *ApJ.*, 479, L101.
 Ebeling, H., Edge, A.C., Böhringer, H., Allen, S.W., Crawford, C.S., Fabian, A.C., Voges, W., & Huchra, J.P. 1998, *MNRAS*, 301, 881.
 Edge, A.C., & Stewart, G. 1991, *MNRAS*, 252, 428.
 Feigelson, E., & Nelson, P. 1985, *ApJ.*, 293, 192.
 Frenk, C.S. White, S.D.M., Efstathiou, G., & Davis, M. 1990, *ApJ.*, 351, 10.
 Jones, C., & Forman, W. 1978, *Ap.J.*, 224, 1.
 Johnson, M.W., Cruddace, R.G., Ulmer, M.P., Kowalski, M.P., & Wood, K.S. 1983, *ApJ*, 266, 425.
 Leir, A.A., & Van den Bergh, S. 1977, *ApJ Suppl.*, 34, 381.
 Lucey, J.R., 1983, *MNRAS*, 204, 33.
 Kowalski, M.P., Ulmer, M.P., & Cruddace, R.G. 1983, *Ap.J.*, 268, 540.
 Kowalski, M.P., Ulmer, M.P., Cruddace, R.G., & Wood, K. 1984, *ApJS*, 56, 403.
 McHardy, I. 1978, *MNRAS*, 184, 783.
 Scaramella, R., Zamorani, G., Vettolani, G., & Chincarini, G. 1991, *AJ*, 101, 342.
 Schwartz, D. 1978, *Ap.J.*, 220, 8.
 Snowden, S.L., McCammon, D., Burrows, D.N., & Mendenhall, J.A. 1994, *Ap.J.*, 423.
 Stark, A.A., Gammie, C.F., Wilson, R.W., Bally, J., Linke, R.A., Heiles, C., & Hurwitz 1992, *Ap.J.*, Suppl, 79, 77.
 Struble, M.F., & Rood, H.J. 1987, *Ap.J. Supp.*, 63, 555.
 Struble, M.F., & Rood, H.J. 1991, *Ap.J.*, 374, 395.
 Trümper, J. 1983, *Adv. Space Res.*, 2, 241.
 van Haarlem, M., Frenk, C., & White, S. 1997, *MNRAS*, 287, 817.
 White, D., Jones, C., & Forman, W. 1997, *MNRAS*, 292, 419.
 West, M.J. 1989, *ApJ*, 347, 610.

TABLE 1
Cluster Sample

Cluster	α (J2000)	δ (J2000)	N_{gal}	BM type	z	targeted	time (sec)	rate (cts s ⁻¹)	error (cts s ⁻¹)	$f_{0.5-2.0 \text{ keV}}$ (ergs cm ⁻² s ⁻¹)	$L_{0.5-2.0 \text{ keV}}$ (ergs s ⁻¹)	L_{bol} (ergs s ⁻¹)
11	00 12 34.6	-16 29 17	129	III	0.166*	0	3084	0.1210	0.0104	1.54e-12	1.82e+44	6.03e+44
115	00 55 54.8	26 24 31	174	III	0.197	0	19177	0.2182	0.0045	3.02e-12	4.99e+44	2.07e+45
135	01 03 17.6	-22 33 55	100	III	0.198*	0	14997	0.0355	0.0024	4.41e-13	7.59e+43	2.23e+44
192	01 24 17.5	04 28 14	90	I	0.121	0	12095	0.0617	0.0035	8.00e-13	5.18e+43	1.43e+44
222	01 37 33.4	-12 59 26	155	II-III	0.211	1	6515	0.0900	0.0039	1.13e-12	2.17e+44	7.65e+44
223	01 37 55.4	-12 48 57	152	III	0.207	1	6515	0.0859	0.0040	1.08e-12	2.00e+44	6.94e+44
314	02 09 35.0	-12 54 54	96	III	0.188*	0	3851	0.0279	0.0049	3.47e-13	5.39e+43	1.53e+44
401	02 58 58.3	13 34 36	90	I	0.075	1	11712	1.5860	0.0120	2.51e-11	6.01e+44	2.56e+45
426	03 19 48.6	41 30 27	88	II-III	0.018	1	4359	35.0880	0.0969	5.91e-10	8.27e+44	2.89e+45
432	03 24 09.7	-05 48 07	108	II	0.203	0	5536	0.0441	0.0039	5.89e-13	1.06e+44	3.27e+44
448	03 38 36.4	-11 10 28	80	III	0.180*	0	8670	0.0628	0.0040	8.34e-13	1.18e+44	3.76e+44
478	04 13 25.4	10 27 54	104		0.088	1	21271	1.6508	0.0089	2.79e-11	9.26e+44	3.65e+45
494	04 30 53.8	-07 46 10	115	III	0.170*	0	6755	0.0260	0.0033	3.61e-13	4.61e+43	1.31e+44
520	04 54 09.4	02 55 15	186	III	0.197	1	4610	0.2546	0.0076	3.75e-12	6.17e+44	2.68e+45
530	05 00 46.2	-00 51 58	86		0.238*	0	7352	0.0586	0.0038	8.37e-13	2.05e+44	7.17e+44
536	05 07 40.5	-09 16 00	97	III	0.040	0	23118	0.1574	0.0068	2.21e-12	1.53e+43	3.67e+43
545	05 32 25.3	-11 32 35	234	III	0.154	1	13280	0.3452	0.0052	5.55e-12	5.60e+44	2.37e+45
563	-	-	84	III	0.139*	0	3995	<0.0120	0.0030	<1.19e-13	<1.04e+43	<2.44e+43
571	07 19 09.5	71 51 13	84	II	0.182*	0	16470	0.0234	0.0021	3.06e-13	4.52e+43	1.23e+44
574	07 20 18.1	70 56 57	102	III	0.174*	0	16470	0.0089	0.0018	1.15e-13	1.59e+43	3.83e+43
586	07 32 19.8	31 37 52	190	I	0.171	1	5334	0.2796	0.0086	3.93e-12	4.89e+44	2.03e+45
625W	08 26 17.9	82 18 27	107	III	0.128*	1	2033	0.1098	0.0083	1.42e-12	1.02e+44	3.11e+44
625E	08 31 40.0	82 22 39	107	III	0.128*	1	2033	0.0441	0.0059	5.66e-13	4.09e+43	1.10e+44
665	08 30 59.1	65 50 43	321	III	0.182	1	33510	0.3590	0.0033	4.86e-12	6.82e+44	3.01e+45
686	08 47 41.9	77 40 52	97	III	0.197*	0	5030	0.0701	0.0059	8.91e-13	1.50e+44	4.91e+44
754	09 09 20.6	-09 40 35	92	I-II	0.053	1	8264	2.4626	0.0184	3.37e-11	4.11e+44	1.92e+45
764	09 17 02.1	63 47 24	82	II-III	0.166*	0	5796	0.0429	0.0040	5.67e-13	6.84e+43	1.97e+44
777	-	-	210	III	0.221	1	6087	<0.0076	0.0019	<6.69e-14	<1.51e+43	<3.62e+43
782	09 21 38.9	52 02 38	107	III	0.176*	0	8464	0.0242	0.0034	2.95e-13	4.04e+43	1.08e+44
787	09 28 44.5	74 23 17	106	II	0.135	0	11923	0.0232	0.0026	2.87e-13	2.34e+43	5.88e+43

Cluster	α (J2000)	δ (J2000)	N_{gal}	BM type	z	targeted	time (sec)	rate (cts s ⁻¹)	error (cts s ⁻¹)	$f_{0.5-2.0 \text{ keV}}$ (ergs cm ⁻² s ⁻¹)	$L_{0.5-2.0 \text{ keV}}$ (ergs s ⁻¹)	L_{bol} (ergs s ⁻¹)
873	-	-	133	III	0.182	0	13442	<0.0053	0.0013	<6.77e-14	<1.03e+43	<2.43e+43
914	10 09 21.2	71 10 28	114	III	0.195	0	8171	0.1126	0.0055	1.50e-12	2.44e+44	8.76e+44
963	10 17 07.0	39 02 28	134	I-II	0.206	0	8878	0.2218	0.0074	2.78e-12	5.01e+44	2.09e+45
968	10 21 03.1	68 14 52	119	III	0.195	0	16652	0.0114	0.0017	1.43e-13	2.46e+43	6.28e+43
981	10 24 17.5	68 05 03	126	III	0.202	0	16652	0.0362	0.0019	4.60e-13	8.21e+43	2.45e+44
998	10 26 25.9	67 55 26	123	II	0.203	1	16652	0.0102	0.0013	1.26e-13	2.35e+43	5.95e+43
1005	10 27 32.3	68 11 36	81	III	0.201	0	16652	0.0067	0.0013	8.13e-14	1.50e+43	3.54e+43
1035	10 32 18.2	40 15 58	94	II-III	0.080	0	4262	0.2092	0.0150	2.57e-12	7.13e+43	2.06e+44
1046	-	-	108	III	0.190	0	8901	<0.0068	0.0017	<6.09e-14	<1.01e+43	<2.37e+43
1049	-	-	108	III	0.258	0	8901	<0.0052	0.0013	<4.68e-14	<1.44e+43	<3.47e+43
1061	10 40 46.0	67 13 53.0	99	III	0.189	1	8901	0.0300	0.0022	3.71e-13	5.85e+43	1.65e+44
1186	11 13 59.1	75 26 13	107	II-III	0.080	1	2362	0.0529	0.0071	6.84e-13	1.92e+43	4.72e+43
1190	11 11 40.8	40 50 02	87	II	0.079	0	13624	0.2960	0.0064	3.68e-12	1.00e+44	3.06e+44
1234	11 22 26.1	21 26 55	88	III	0.166	0	32843	0.0376	0.0019	4.60e-13	5.61e+43	1.58e+44
1240	11 23 37.6	43 05 51	102	III	0.159*	0	13821	0.0643	0.0030	8.11e-13	8.96e+43	2.71e+44
1259	-	-	100	II-III	0.226*	0	2134	<0.0176	0.0044	<1.74e-13	<3.97e+43	<1.06e+44
1302	11 33 14.2	66 22 56	85	II	0.117	1	2260	0.2283	0.0109	2.81e-12	1.65e+44	5.47e+44
1351	11 42 33.0	58 32 28	96	I-II	0.322	0	3918	0.0902	0.0094	1.12e-12	4.93e+44	2.07e+45
1367	11 44 41.0	19 42 36	117	II-III	0.021	1	17265	3.0322	0.0166	3.82e-11	7.55e+43	2.14e+44
1381	11 48 41.6	75 15 55	92	II-III	0.117	1	2009	0.0422	0.0058	5.49e-13	3.32e+43	8.67e+43
1401	11 51 52.9	37 16 12	153	III	0.165	0	2234	0.0553	0.0075	6.92e-13	8.22e+43	2.44e+44
1413	11 55 18.4	23 24 15	196	I	0.143	1	7189	0.5643	0.0090	7.22e-12	6.24e+44	2.85e+45
1446	12 02 04.9	58 02 38	85	II-III	0.103	1	5184	0.1563	0.0063	1.94e-12	9.01e+43	2.71e+44
1455	-	-	91	II	0.155*	0	23035	<0.0109	0.0027	<1.32e-13	<1.44e+43	<3.45e+43
1469	12 05 45.6	-07 07 06	84	III	0.152*	0	8962	0.0365	0.0031	4.68e-13	4.79e+43	1.31e+44
1470	12 06 55.6	71 39 10	93	III	0.192	0	3304	0.0663	0.0056	8.25e-13	1.32e+44	4.24e+44
1489	-	-	99	II	0.206*	0	2063	<0.0124	0.0031	<1.52e-13	<2.93e+43	<7.35e+43
1497	12 14 15.1	26 38 49	101	II-III	0.167	0	2982	0.0414	0.0062	5.14e-13	6.30e+43	1.80e+44
1504	12 15 23.6	27 29 06	98	I-II	0.184	0	2063	0.0379	0.0066	4.71e-13	6.99e+43	2.03e+44
1510	12 16 38.8	27 11 15	80	II-III	0.215*	0	2982	0.0204	0.0048	2.53e-13	5.20e+43	1.44e+44

David et al.

Cluster	α (J2000)	δ (J2000)	N_{gal}	BM type	z	targeted	time (sec)	rate (cts s ⁻¹)	error (cts s ⁻¹)	$f_{0.5-2.0 \text{ keV}}$ (ergs cm ⁻² s ⁻¹)	$L_{0.5-2.0 \text{ keV}}$ (ergs s ⁻¹)	L_{bol} (ergs s ⁻¹)
1515	-	-	81	III	0.181*	0	13943	<0.0112	0.0028	<1.00e-13	<1.50e+43	<3.60e+43
1539	12 26 02.7	62 32 08	96	III	0.171	1	2284	0.0265	0.0042	3.28e-13	4.26e+43	1.15e+44
1546	-	-	86	III	0.234	0	4057	<0.0120	0.0030	<1.48e-13	<3.63e+43	<9.59e+43
1550	12 29 04.7	47 37 28	167	III	0.254	0	4794	0.0688	0.0054	8.50e-13	2.36e+44	8.48e+44
1557	12 32 36.3	62 52 51	89	III	0.210	0	14978	0.0459	0.0024	5.72e-13	1.11e+44	3.45e+44
1560	12 33 55.5	15 11 05	123		0.244*	0	592	0.1171	0.0163	1.50e-12	3.83e+44	1.51e+45
1565	12 35 07.1	41 17 51	85	III	0.183*	0	2263	0.0236	0.0054	2.91e-13	4.32e+43	1.17e+44
1566	-	-	91	III	0.101	1	2158	<0.0299	0.0075	<3.66e-13	<1.64e+43	<3.96e+43
1576	12 36 58.9	63 11 12	158	I	0.302	1	14978	0.1201	0.0029	1.52e-12	5.86e+44	2.55e+45
1607	-	-	82	III	0.136	1	2204	<0.0116	0.0029	<1.06e-13	<8.90e+42	<2.06e+43
1636	12 53 07.9	62 48 25	103	III	0.235	0	6668	0.0225	0.0024	2.79e-13	6.82e+43	2.00e+44
1656	12 59 35.2	27 56 55	106	II	0.023	1	20572	13.500	0.0293	1.68e-10	3.86e+44	1.69e+45
1664	13 03 42.2	-24 14 54	112		0.169*	1	12299	0.3867	0.0059	5.85e-12	7.12e+44	3.17e+45
1689	13 11 29.3	-01 20 29	228	II-III	0.183	1	12989	0.6553	0.0071	8.35e-12	1.18e+45	5.85e+45
1706	-	-	92	III	0.156*	0	14855	<0.0088	0.0022	<7.67e-14	<8.53e+42	<1.95e+43
1758N	13 32 44.8	50 32 23.9	198	III	0.280	1	14932	0.1572	0.0034	1.95e-12	6.46e+44	2.86e+45
1758S	13 32 32.8	50 24 48.4	198	III	0.280	1	14932	0.1163	0.0029	1.44e-12	4.79e+44	1.99e+45
1763	13 35 18.6	40 59 54	152	III	0.187	1	12335	0.2469	0.0046	3.05e-12	4.55e+44	1.81e+45
1775	13 41 49.8	26 22 02	92	I	0.072	0	7772	0.5813	0.0102	7.16e-12	1.59e+44	5.25e+44
1795	13 48 52.8	26 35 26	115	I	0.062	1	33589	2.9239	0.0097	3.62e-11	6.02e+44	2.07e+45
1838	-	-	130	II-III	0.248	0	1369	<0.0280	0.0070	<3.40e-13	<9.18e+43	<2.79e+44
1904	14 22 13.3	48 30 20	83	II-III	0.071	1	3020	0.1793	0.0097	2.23e-12	4.86e+43	1.33e+44
1914	14 26 01.1	37 49 26	105	II	0.171	1	6065	0.6502	0.0104	8.09e-12	1.00e+45	4.80e+45
1937	14 34 37.1	58 16 06	99	III	0.138	0	3516	0.0256	0.0041	3.11e-13	2.64e+43	6.71e+43
1940	14 35 24.8	55 07 33	130	III	0.140	1	2679	0.1081	0.0071	1.33e-12	1.13e+44	3.52e+44
2008	-	-	93	II	0.181	0	4264	<0.0212	0.0053	<2.73e-13	<3.99e+43	<1.04e+44
2029	15 10 56.1	05 44 36	82	I	0.077	1	9604	2.9320	0.0179	3.85e-11	9.69e+44	4.13e+45
2034	15 10 12.6	33 30 32	105	II-III	0.140*	1	6985	0.5002	0.0087	6.29e-12	5.24e+44	2.19e+45
2069	15 24 11.3	29 52 14	97	II-III	0.116	0	3291	0.3024	0.0133	3.83e-12	2.21e+44	7.78e+44
2104	15 40 08.7	-03 19 07	89	III	0.169*	0	8070	0.2395	0.0077	3.57e-12	4.35e+44	1.75e+45

Cluster	α (J2000)	δ (J2000)	N_{gal}	BM type	z	targeted	time (sec)	rate (cts s ⁻¹)	error (cts s ⁻¹)	$f_{0.5-2.0 keV}$ (ergs cm ⁻² s ⁻¹)	$L_{0.5-2.0 keV}$ (ergs s ⁻¹)	L_{bol} (ergs s ⁻¹)
2111	15 39 41.0	34 25 07	148	II-III	0.229	1	6455	0.1385	0.0048	1.76e-12	3.93e+44	1.56e+45
2125	15 41 02.1	66 16 17	230	II-III	0.246	1	13772	0.0333	0.0017	4.30e-13	1.14e+44	3.59e+44
2142	15 58 19.8	27 13 45	89	II	0.090	1	4662	2.3723	0.0228	3.18e-11	1.10e+45	4.97e+45
2151	16 04 35.5	17 43 36	87	III	0.037	1	10820	0.9424	0.0163	1.23e-11	7.19e+43	2.11e+44
2163	16 15 45.8	-06 08 51	119		0.203	1	11112	0.5788	0.0073	9.29e-12	1.60e+45	9.52e+45
2198	-	-	85	III	0.080	1	2126	<0.0252	0.0063	<2.92e-13	<8.37e+42	<1.89e+43
2199	16 28 38.2	39 33 00	88	I	0.030	1	34586	5.0750	0.0248	6.21e-11	2.39e+44	7.59e+44
2201	16 26 58.7	55 28 27	95	I-II	0.133	0	3377	0.1471	0.0085	1.83e-12	1.41e+44	4.52e+44
2204	16 32 47.2	05 34 22	133	II	0.152	1	4978	1.0701	0.0150	1.50e-11	1.47e+45	7.62e+45
2218	16 35 52.0	66 12 37	214	II	0.171	1	35374	0.2793	0.0029	3.68e-12	4.59e+44	1.87e+45
2219	16 40 21.1	46 41 59	159	III	0.186*	1	8191	0.4785	0.0077	6.07e-12	8.88e+44	4.15e+45
2244	17 02 41.5	34 03 31	89	I-II	0.097	1	2862	0.8827	0.0180	1.12e-11	4.52e+44	1.82e+45
2246W	17 00 41.1	64 13 07	146	II-III	0.225	0	33221	0.0324	0.0010	4.12e-13	9.17e+43	2.77e+44
2246E	17 01 21.8	64 14 20	146	II-III	0.225	0	33221	0.0255	0.0010	3.24e-13	7.24e+43	2.11e+44
2255	17 12 41.8	64 03 59	102	II-III	0.080	1	11274	0.7008	0.0083	9.08e-12	2.49e+44	1.02e+45
2256	17 03 36.5	78 39 05	88	II-III	0.058	1	16913	2.2647	0.0123	3.06e-11	4.43e+44	1.84e+45
2291	17 56 55.9	51 09 36	82		0.181*	0	15885	0.0192	0.0022	2.50e-13	3.67e+43	9.73e+43
2302	18 19 58.2	57 09 33	119	III	0.179*	0	4464	0.0785	0.0058	1.04e-12	1.45e+44	4.74e+44
2316	-	-	85	II-III	0.167*	0	14523	<0.0126	0.0032	<1.66e-13	<2.08e+43	<5.31e+43
2317	19 08 16.6	69 03 22	186	II	0.211	0	12547	0.0668	0.0033	9.48e-13	1.82e+44	6.22e+44
2354	21 35 35.3	-14 59 19	81	III	0.144*	0	4580	0.0541	0.0090	7.29e-13	6.67e+43	1.88e+44
2355	21 35 11.4	01 24 34	112	III	0.124	0	5816	0.1308	0.0100	1.75e-12	1.18e+44	3.68e+44
2356	21 35 43.0	00 08 44	89	II-III	0.116	0	5816	0.1025	0.0066	1.36e-12	8.00e+43	2.35e+44
2387	21 37 26.4	83 07 07	101		0.145*	0	4583	0.0148	0.0036	2.09e-13	1.96e+43	4.84e+43
2397	21 56 08.8	01 23 27	146	I	0.224	1	12695	0.1091	0.0031	1.51e-12	3.25e+44	1.24e+45
2507	22 56 49.7	05 30 36	92	II-III	0.196	1	4841	0.0867	0.0045	1.21e-12	1.97e+44	9.34e+44
2670	23 54 12.6	-10 25 10	142	I-II	0.076	1	14476	0.4409	0.0061	5.65e-12	1.42e+44	4.21e+44
2744	00 14 19.0	-30 23 12	137	III	0.308	1	13173	0.2066	0.0040	2.65e-12	1.05e+45	5.17e+45
3093	03 10 52.6	-47 24 19	93	I	0.059	1	7554	0.0487	0.0057	5.96e-13	9.00e+42	2.08e+43
3112	03 17 57.8	-44 14 18	116	I	0.070	1	6800	1.3669	0.0148	1.73e-11	3.69e+44	1.12e+45

Cluster	α (J2000)	δ (J2000)	N_{gal}	BM type	z	targeted	time (sec)	rate (cts s ⁻¹)	error (cts s ⁻¹)	$f_{0.5-2.0 \text{ keV}}$ (ergs cm ⁻² s ⁻¹)	$L_{0.5-2.0 \text{ keV}}$ (ergs s ⁻¹)	L_{bol} (ergs s ⁻¹)
3128	03 29 51.5	-52 35 07	140	I-II	0.055	1	9657	0.5432	0.0103	6.90e-12	9.14e+43	2.74e+44
3135	03 34 01.7	-39 00 54	111	II	0.051*	0	20796	0.0922	0.0040	1.14e-12	1.29e+43	3.10e+43
3139	03 36 35.7	-23 40 11	100	II-III	0.239*	0	17288	0.0428	0.0024	5.41e-13	1.35e+44	4.37e+44
3158	03 42 53.5	-53 37 50	85	I-II	0.060	1	2826	1.5788	0.0253	1.99e-11	3.10e+44	1.09e+45
3223	04 08 19.3	-31 00 20	100	I	0.061	1	7339	0.3247	0.0080	3.97e-12	6.56e+43	1.87e+44
3259	04 28 49.7	-38 06 07	130	III	0.141*	0	3353	0.0174	0.0035	2.14e-13	1.91e+43	4.69e+43
3263	-	-	94	III	0.146*	0	3353	<0.0128	0.0032	<1.17e-13	<1.12e+43	<2.65e+43
3266	04 31 19.4	-61 26 50	91	I-II	0.059	1	19473	2.2075	0.0114	2.84e-11	4.31e+44	1.61e+45
3297	04 58 29.5	-30 08 31	112	III	0.106*	0	7246	0.0579	0.0049	7.22e-13	3.56e+43	9.37e+43
3301	05 00 49.6	-38 40 21	172	I	0.055	1	8152	0.3892	0.0091	4.88e-12	6.31e+43	1.79e+44
3305	05 01 55.3	-39 12 58	85	I-II	0.192*	0	8152	0.0217	0.0025	2.71e-13	4.43e+43	1.20e+44
3312	-	-	118	III	0.106*	0	505	<0.0636	0.0159	<5.89e-13	<2.94e+43	<7.54e+43
3360	05 40 40.0	-43 27 02	85	III	0.084	0	2381	0.1740	0.0144	2.29e-12	7.14e+43	2.07e+44
3426	-	-	80	III	0.237*	0	3674	<0.0108	0.0027	<1.32e-13	<3.35e+43	<8.78e+43
3438	10 15 03.3	-28 33 22	111	II-III	0.248*	0	4297	0.0172	0.0038	2.41e-13	6.58e+43	1.90e+44
3440	10 16 01.3	-29 21 46	155	II-III	0.240*	0	4297	0.0117	0.0028	1.64e-13	4.25e+43	1.15e+44
3471	11 11 11.9	-30 09 43	103	II-III	0.196*	0	6360	0.0860	0.0059	1.25e-12	2.08e+44	7.26e+44
3558	13 27 56.6	-31 29 42	226	I	0.048	1	26974	2.5862	0.0109	3.47e-11	3.48e+44	1.02e+45
3559	13 29 53.1	-29 30 22	141	I	0.047	1	7544	0.1426	0.0086	1.89e-12	1.83e+43	4.46e+43
3560	13 32 26.5	-33 08 38	184	I	0.049	1	5106	0.5940	0.0385	7.64e-12	8.10e+43	2.76e+44
3562	13 33 36.1	-31 40 21	129	I	0.050	1	17018	1.0988	0.0102	1.48e-11	1.59e+44	4.67e+44
3566	13 39 24.0	-35 35 37	100	II	0.048	1	6895	0.0422	0.0100	5.67e-13	5.82e+42	1.31e+43
3571	13 47 29.0	-32 51 24	126	I	0.040	1	4955	4.7161	0.0370	6.63e-11	4.48e+44	1.79e+45
3576	13 52 39.0	-30 16 34	110	I	0.149*	0	7880	0.0209	0.0035	2.82e-13	2.78e+43	7.10e+43
3667	20 12 33.0	-56 50 30	85	I-II	0.054	1	11156	2.3359	0.0161	3.28e-11	4.10e+44	1.58e+45
3735	-	-	89	III	0.156*	0	12715	<0.0124	0.0031	<1.81e-13	<1.30e+43	<3.10e+43
3818	-	-	118	II-III	0.154*	0	24246	<0.0048	0.0012	<4.17e-14	<4.55e+42	<1.02e+43
3829	-	-	88	III	0.214*	0	9240	<0.0092	0.0023	<8.14e-14	<1.70e+43	<4.15e+43
3834	22 05 38.8	-47 28 17	154	III	0.157*	0	8439	0.0295	0.0037	3.65e-13	3.99e+43	1.06e+44
3839	-	-	115	II	0.128*	0	3512	<0.0220	0.0055	<2.68e-13	<1.97e+43	<4.72e+43
3888	22 34 26.7	-37 44 00	107	I-II	0.168	0	4093	0.4597	0.0110	5.76e-12	6.90e+44	3.06e+45
3921	22 49 59.2	-64 25 43	93	II	0.087*	1	11154	0.5990	0.0077	7.65e-12	2.47e+44	8.84e+44
4038	23 47 43.5	-28 08 22	117	III	0.028	1	2887	2.6564	0.0370	3.30e-11	1.14e+44	3.16e+44

Notes: This table gives the ACO cluster number, X-ray centroid, number of cluster members between m_3 and $m_3 + 2$ (N_{gal}), Bautz-Morgan Type, redshift, a flag to indicate whether the cluster was part of a targeted observation (1) or was observed serendipitously (0), screened integration time, 0.5-2.0 keV PSPC count rate or 4σ upper limit, 1σ error in the PSPC count rate, unabsorbed 0.5-2.0 keV flux, rest frame 0.5-2.0 keV X-ray luminosity, and rest frame bolometric luminosity. All distant dependent quantities are computed assuming $H_0 = 50 \text{ km}^{-1} \text{ s}^{-1} \text{ Mpc}^{-1}$ and $q_0 = 0.5$.

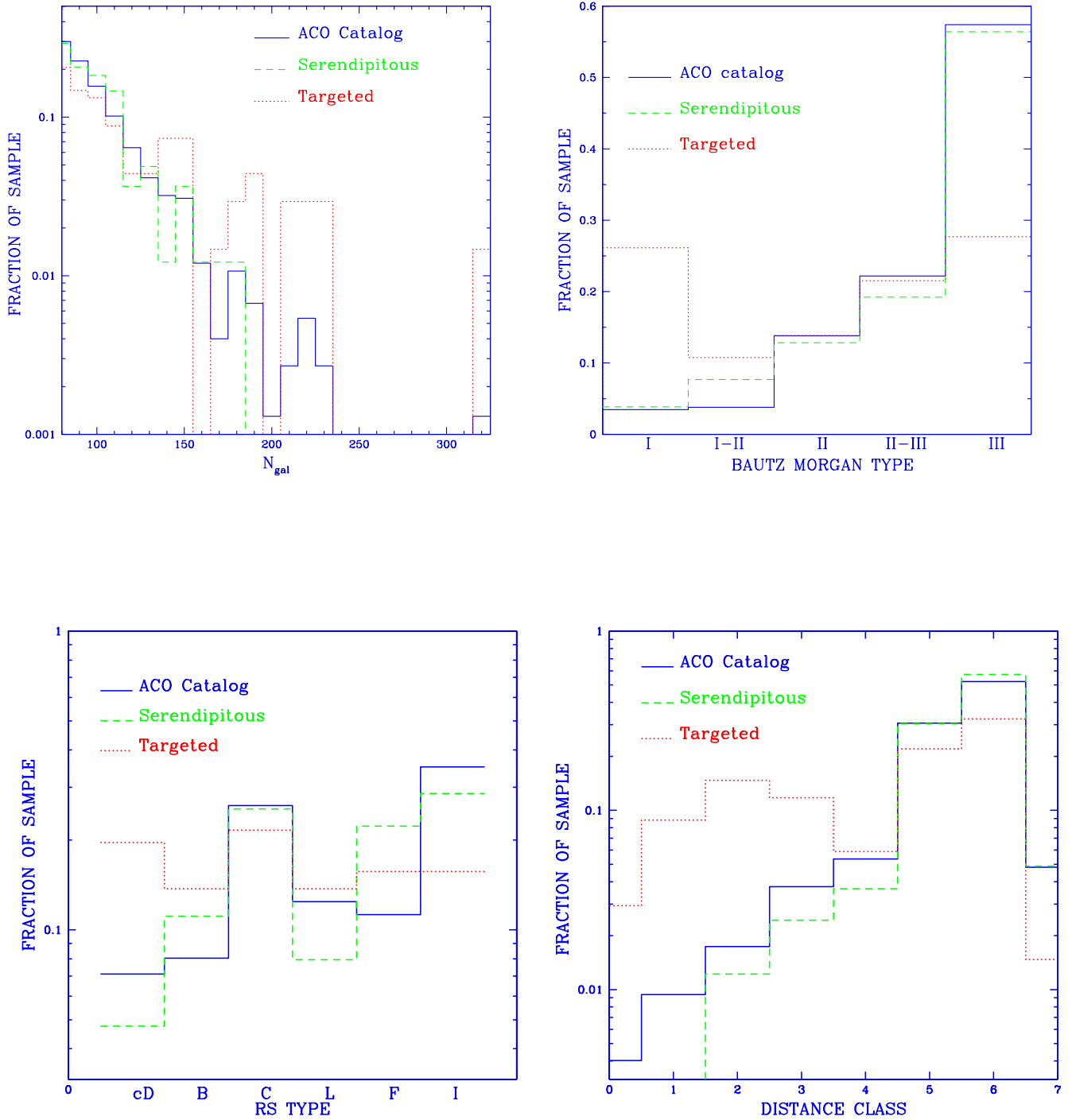


FIG. 1. Comparison of the optical properties of clusters in the ACO catalog with the optical properties of clusters observed with the PSPC. The PSPC sample is divided into serendipitously observed clusters and targeted observations. Comparisons are shown between a) cluster richness (N_{gal}), b) Bautz Morgan Type, c) Rood Sastry Type, and d) distance class.

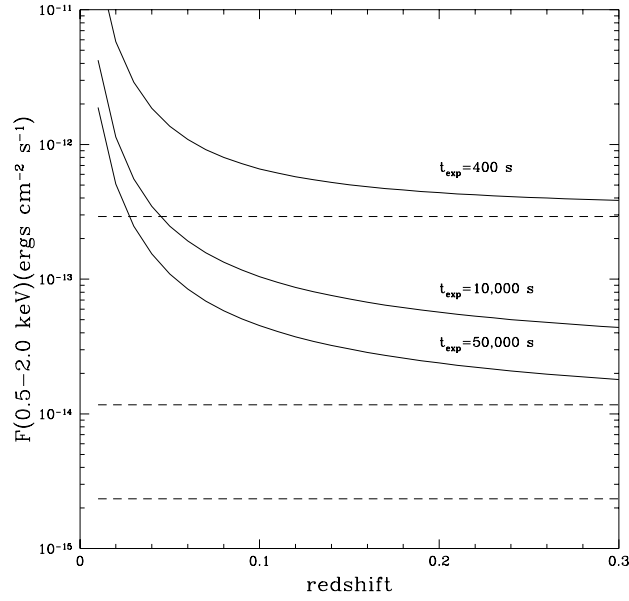


FIG. 2. Typical 3σ flux limits for extended sources (solid lines) at several representative PSPC exposure times as a function of redshift (see the text for details). Also shown in the corresponding 3σ flux limit for point sources (dashed lines).

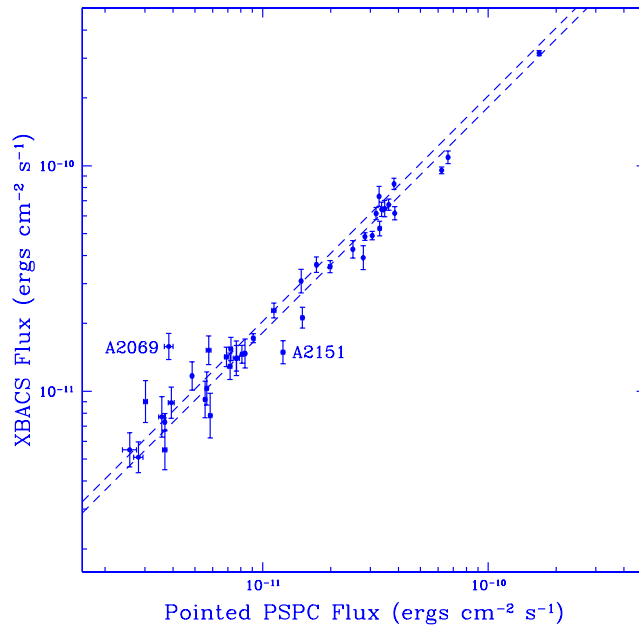


FIG. 3. A comparison of the measured fluxes for $R \geq 2$ clusters in XBACS that were also observed during pointed PSPC observations. The XBACS flux is the total 0.1-2.4 keV flux given in Ebeling *et al.* (1996) and the pointed PSPC flux is the 0.5-2.0 keV flux within the central 1 Mpc listed in Table 3. The dashed lines indicate exact agreement under the assumption of a spherically symmetric β model for clusters with core radii of 100 kpc (lower line) and 250 kpc (upper line). The two most discrepant clusters are identified in the plot.

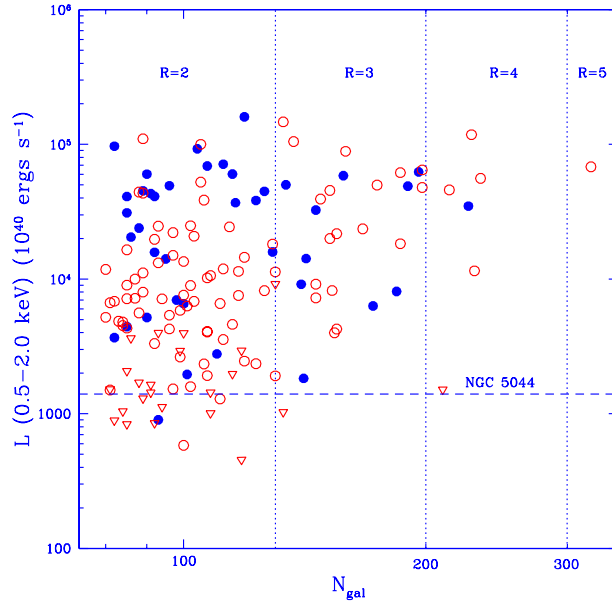


FIG. 4. Scatter plot of X-ray luminosity vs. cluster richness (N_{gal}) for the entire sample. Early Bautz Morgan Type clusters are shown as filled symbols and late Bautz Morgan Type clusters are shown as open symbols. Detections are shown as circles and upper limits are shown as triangles.

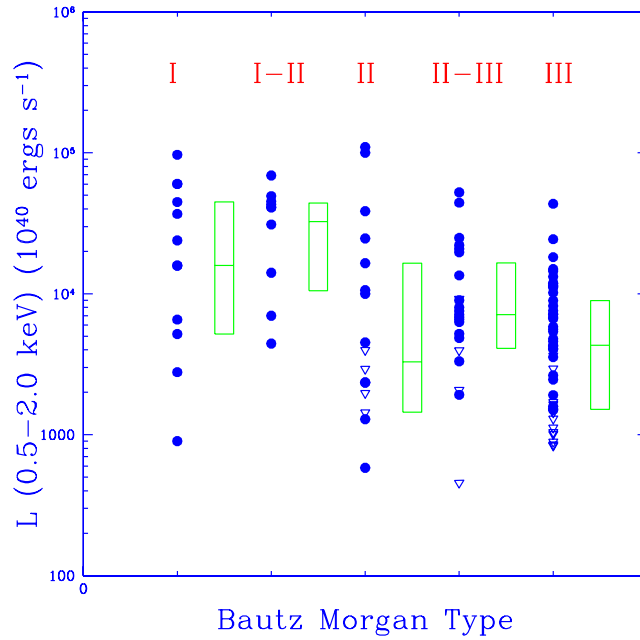


FIG. 5. Scatter plot of X-ray luminosity vs. Bautz Morgan Type for R=2 clusters. Detections are shown as circles and upper limits are shown as triangles. Also shown are the 25, 50, and 75% percentiles for each Bautz Morgan Type.

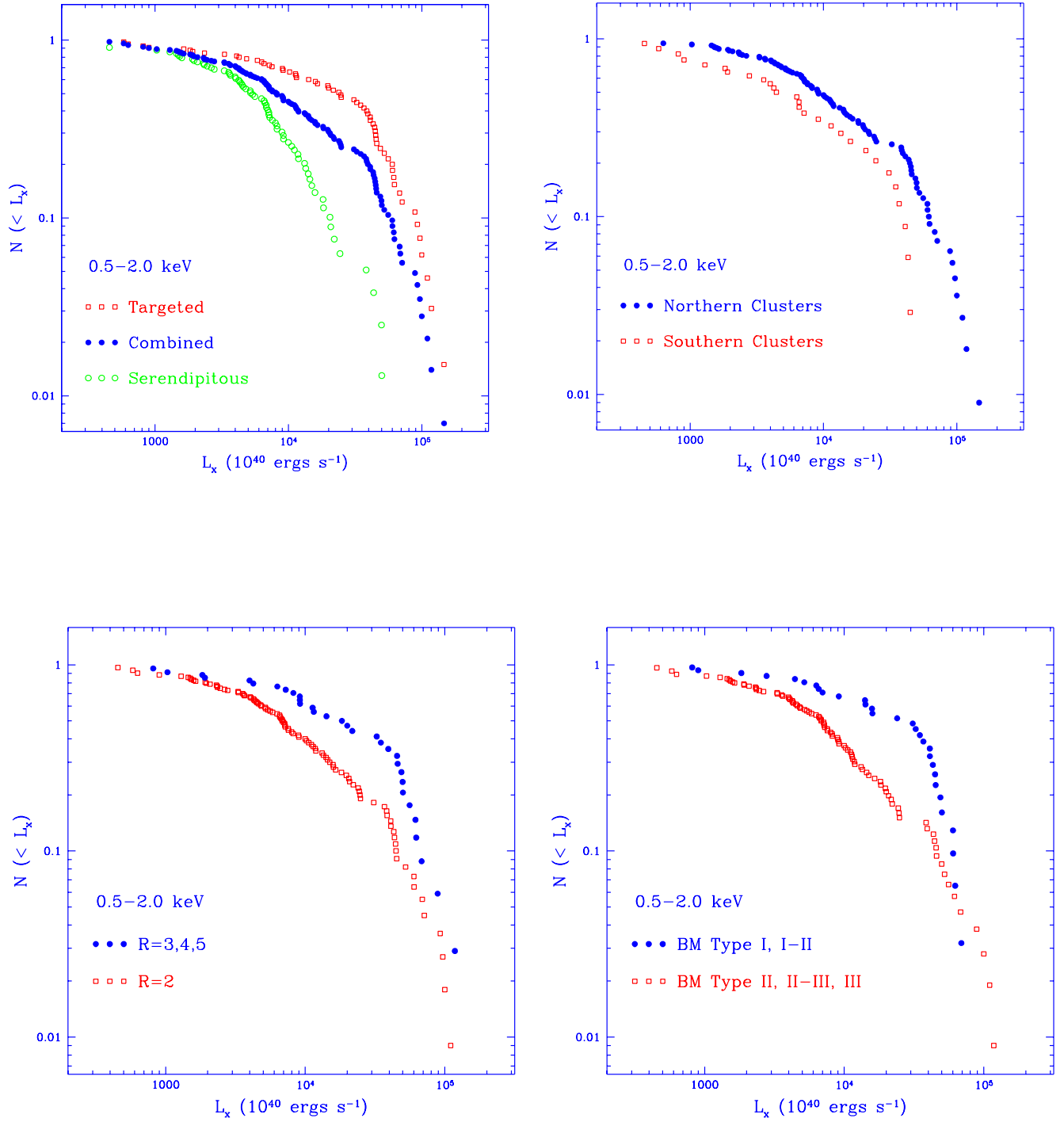


FIG. 6. Comparison of the 0.5-2.0 keV luminosity function for different sub samples. a) serendipitous vs. targeted samples, b) Abell vs. southern ACO, c) richness class ($R=2$ vs. $R=3,4$, and $R=5$), and d) Bautz Morgan Types (early vs. late).

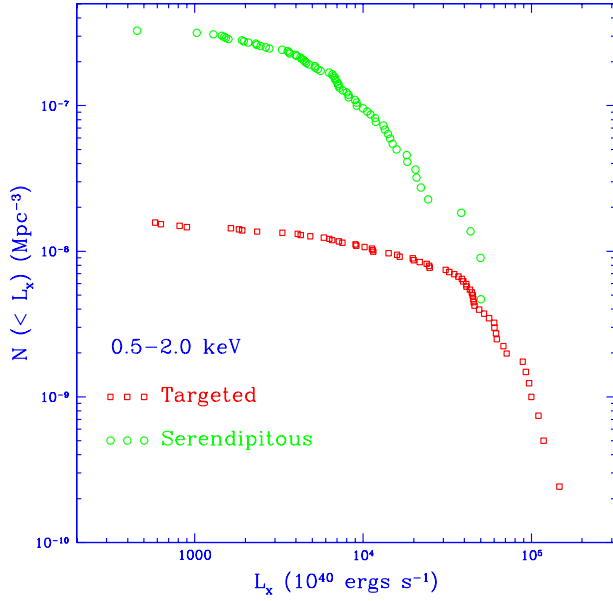


FIG. 7. Luminosity functions of the volume normalized targeted sample and ACO number density normalized serendipitous sample.

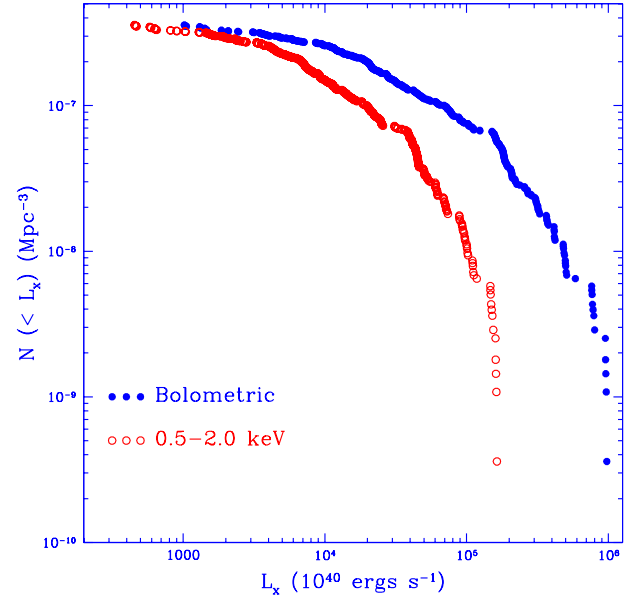


FIG. 8. Bolometric and 0.5-2.0 keV luminosity function of the entire PSPC sample normalized using the technique described in the text.

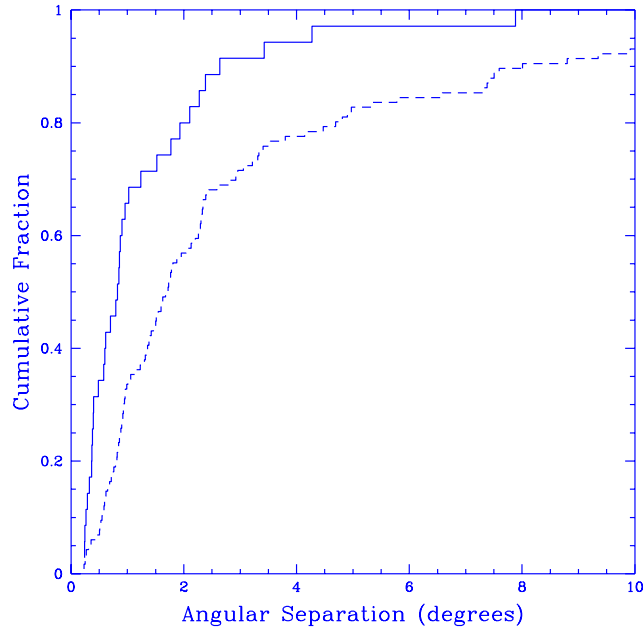


FIG. 9. The cumulative distribution of the angular separations between clusters in the PSPC sample and their nearest neighboring Abell or ACO cluster. Only clusters with $\Delta m_{10} \leq 0.2$ are considered. The solid line corresponds to low X-ray luminosity clusters ($L(0.5 - 2.0 \text{ keV}) < 3.0 \times 10^{43} \text{ ergs s}^{-1}$) and the dashed lines corresponds to more luminous clusters.